Using RANS computations to calculate support interference effects on the Common Research Model

Aurélia Cartieri, David Hue
ONERA CS 70100, 8 rue des Vertugadins
73500 Modane, 92180 Meudon
France

aurelia.cartieri@onera.fr, david.hue@onera.fr

ABSTRACT

Experimental aerodynamic investigations of the NASA Common Research Model and the ONERA Large Reference Model, which is a 220% scaled copy of the Common Research Model, have been conducted in the NASA Langley National Transonic Facility, the NASA Ames 11-ft wind tunnel the European Transonic Wind Tunnel and the ONERA-S1MA wind tunnel. To improve the accuracy of flight data prediction from measurement data in the wind tunnel, the evaluation of the various bias of the experimental simulations in the wind tunnel has to be made. One of the applications is the support interference effect. Effects of the support interference are studied by means of steady RANS simulations of the flow. The support interference correction method is applied to the wind tunnel data. Special attention was paid to the proper derivation of corrections of the incoming flow conditions in terms of Mach number and angle of attack. Additional forces corrections have been calculated and results from different wind tunnels and different support can be compared.

1.0 INTRODUCTION

The Common Research Model (CRM) developed by NASA and Boeing [1][2] serves as a reference for providing wind tunnel data aimed at the validation of codes dedicated to aircraft performance prediction. This model has been designed and built as part of the AIAA Drag Prediction Workshop (DPW) series [3]. Recently, ONERA has built its own CRM model; it is the Large Reference Model (LRM). It has been designed to have the same geometry as the NASA model when submitted to equivalent constraints. The ONERA model will be used to verify the complete measurement chain of the SIMA facility [4], which is one of the greatest transonic wind tunnels in the world. These verifications will concern the wind tunnel structure itself (for instance after repairs and modifications), quality of the airstream, checkouts of data repeatability over time. Moreover, in the meantime, this model is also used for technical development of new measurement techniques and devices as well as a reference for Computational Fluid Dynamics (CFD) validation at ONERA.

At the end of 2014, the first test campaign involving the LRM took place in S1MA. The main purpose of this test was to acquire a large reference database on this model. Since then, several campaigns have been carried out. Comparisons between wind tunnels can be made [5], introducing CRM data from other wind tunnels such as NASA National Transonic Facility (NTF), Ames, and also the European Transonic Wind tunnel (ETW) [6]. For this matter, support interference effects are introduced as it is generally recognised that aerodynamic interference caused by the model support may have a significant effect on the measured data and several studies were undertaken in the past decades [7][8] to determine this effect for numerous configurations and flow velocity.

2.0 WIND TUNNEL TESTS

2.1 Facility description

2.1.1 S1MA

S1MA is a continuous atmospheric wind tunnel operating in the sub/transonic regime. It was put into service in 1952 and is equipped with two contra-rotating fans, driven by Pelton turbines, the power of which is 88 MW. The wind velocity can be varied from a few meters per second to approximately Mach 1 by varying the fan speed. The total length of the aerodynamic circuit is about 400 m (see **Figure 1**). The test section dimensions are 14m in length and 8m in diameter. For a Mach number around 0.85, the Reynolds number per meter is about 11 million.

A peculiarity of the circuit is the absence of heat exchanger. The temperature is controlled by letting outside fresh air enter the circuit. Hot air naturally exhausts around the edge of the contraction through an annular exit. An exhaust rate of about 10% of the total mass flow is required to maintain a temperature of about 50°C in the tunnel.
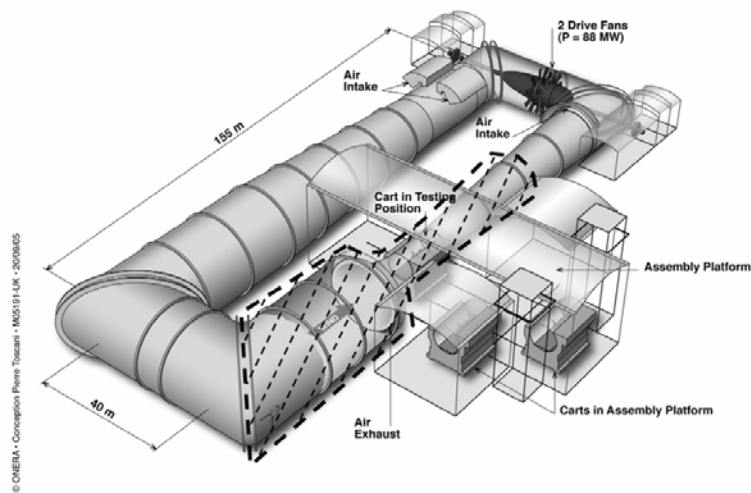
Figure 1: S1MA air circuit.

2.1.2 Other wind tunnels

The NASA National Transonic Facility (NTF), the NASA Ames 11-ft Transonic wind Tunnel and the European Transonic Wind tunnel (ETW) are detailed in [9].

2.2 Model description

2.2.1 ONERA model

The model used in the current investigation is the ONERA Large Reference Model (LRM) which has the same geometry as the NASA Common Research Model (CRM). It was sized to 220% of the NASA model, so the final scale is 1/16.835. This configuration consists of a contemporary supercritical transonic wing ($AR = 9.0$) and a fuselage that are representative of a wide-body commercial transport aircraft. The vertical tail geometry was designed by the Civil Aircraft Unit of the Applied Aerodynamics Department in cooperation with the Wind Tunnel Division.

The CRM is designed for a cruise Mach number of 0.85 and a corresponding lift coefficient of CL=0.5. The S1 model is defined by mean aerodynamic chord L_{ref} = 0.4161 m, reference surface area S_{ref} = 1.3538 m² and a span b = 3.4905 m.

The ONERA LRM model was designed so that it has the same deformation at cruise point as the CRM model tested in the NTF Wind Tunnel. The main dimensions of the model are given in **Figure 2**.
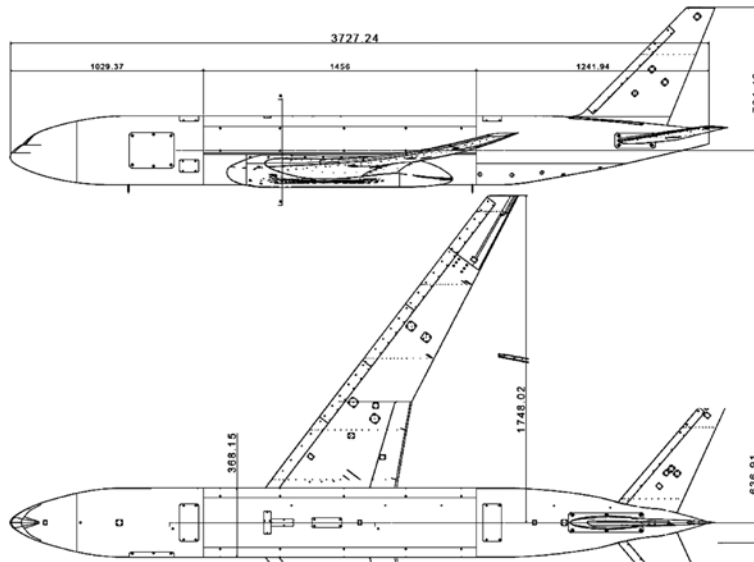
Figure 2: Main dimensions of the LRM model.

Pressure distributions are measured on both the left and right wings using 270 pressure orifices located in nine spanwise stations : five on the right wing (η = 0.131, 0.283, 0.502, 0.727 and 0.950) and four on the left wing (η = 0.201, 0.397, 0.727 and 0.846) . There were also one section on the VTP, and three sections on the HTP (η = 0.2, 0.5 and 0.8). The fuselage was also equipped as shown in **Figure 3**.
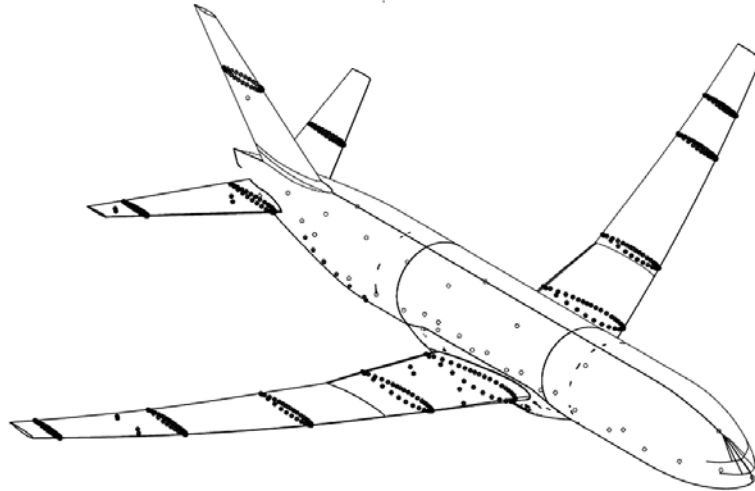
Figure 3: Pressure measurements.

All pressure measurements were made using Electronically Scanned Pressure (ESP) modules installed inside the forward portion of the fuselage. The model is mounted in the wind tunnel using a Z sting setup as shown in **Figure 4**.

Figure 4: The LRM model in S1MA wind tunnel.

2.2.2   CRM model

The CRM model has been tested in several wind tunnels as the NTF, Ames and ETW. The model is mounted in the wind tunnels using a blade sting arrangement in all three wind tunnels, as shown in **Figure 5**.
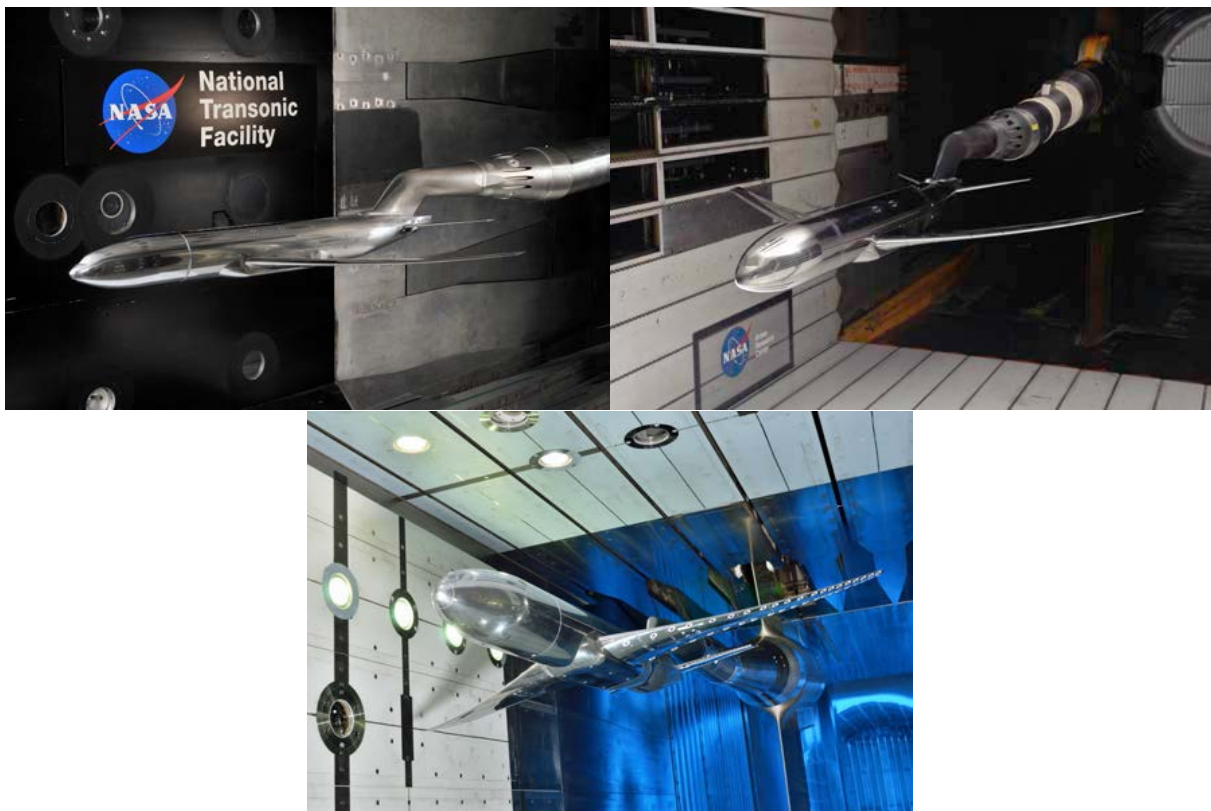
Figure 5: The CRM model in the NTF (top left), the Ames wind tunnel (top right) and the ETW wind tunnel (bottom).

2.3   S1MA test conditions and measurements

The tests in S1MA were carried out in a Mach number range going from $Ma = 0.30$ up to $Ma = 0.95$. The Reynolds number based on mean aerodynamic chord was 5 million. The incidence range was from -3.0° to +10.0°. The incidence of the model was measured by means of three goniometers connected to the weighed balance adapter. It was corrected for wall and sting effects (see below) and for the wind tunnel up-wash that was determined during the campaign. The loads of the model were measured with a six-component balance equipped with two temperature sensors. The wing deformation measurements were performed with two high resolution cameras located in the ceiling of the test section [10] behind a window. The bending and twist deformations of the right wing were derived from the comparison of the 3D target positions between wind-on and wind-off conditions. The deformation measurements obtained at $Ma = 0.85$ and $CL = 0.5$ were in good agreement with the results obtained in NTF and ETW wind tunnels.

The transition of the boundary layer on the different parts of the model was forced by means of Cadcut strips. A cadcut strip consists of an adhesive band on which dots (measuring 1.3 mm in diameter) are precut by a laser at regular intervals (spaced 2.4 mm apart). The trips dost were installed at 10% chord on the wings, the HTP and the VTP. The trip dots were 0.142 mm high on the wing and 0.127 mm high on the tails. On the fuselage, the trips were applied at 60 mm from the nose and measured 0.152 mm. Some acenaphtene visualizations were performed at the beginning of the test campaign in order to check the effectiveness of the boundary layer tripping.

2.4   S1MA correction methods

2.4.1   Basic wind tunnel corrections

The aerodynamic interferences are taken into account thanks to a correction process composed of several contributions:

- The empty test section correction: it is a Mach number. The correction establish the relationship between the Mach number at the wind tunnel reference pressure tap and the Mach number at the reference point of the model measured during the test section calibration (with a probe);

- The buoyancy correction: it is the effect of the empty wind tunnel Mach number gradient on drag (which is proportional to the product of the gradient and the effective volume of the body);

- The sting cavity pressure correction: this correction results from the presence of a pressure coefficient (not zero) inside the rear fuselage which is "open" to enable sting entry. It consists in replacing, on the cavity surface, the mean measured cavity pressure by the reference pressure.

2.4.2   Conventional wall and support corrections

The wall corrections and the conventional support corrections rely on the potential flow theory [11]. Under the assumption that the flow in the tunnel is irrotational outside the boundary layers and wakes, it can be described by a velocity potential $U_{0x} + \varphi$. Assuming now that the velocity perturbations $\partial x\varphi$, $\partial y\varphi$ and $\partial z\varphi$ are small with regard to U_∞, one comes to the well-known linearized potential equation:

$$\left(1 - Ma_\infty^2\right)\partial_x^2\varphi + \partial_y^2\varphi + \partial_z^2\varphi = 0 \quad \textbf{(1)}$$

with boundary conditions at solid walls linearized as well.

Unfortunately, this last assumption is less and less valid as the upstream Mach number Ma_∞ values approach $Ma = 1.00$ and as typical transonic phenomena occur on the model, with large fluid accelerations up to supersonic regime.

This equation and the corresponding boundary conditions can be solved through a distribution of singularities on the model and support. The intensity of each singularity is based on the cross section areas, the lift and the drag.

Once the proper singularities have been set up, the linearity of Eq. (1) allows the potential φ to be broken down into a field φm generated by the model and a field φs generated by the support. Hence $\nabla\varphi s = (us, vs, ws)$ is the field of velocity distortion generated by the support.

Once the velocity field $\nabla \varphi s$ is known, one can easily determine a field of Mach number distortion:

$$\delta Ma = Ma_\infty \left(1 + \frac{\gamma - 1}{2} Ma_\infty^2\right) \frac{u_s}{U_\infty} \quad \textbf{(2)}$$

and a field of angle of attack distortion (upwash):

$$\delta \alpha = \frac{w_s}{U_\infty} \quad \textbf{(3)}$$

These fields are then averaged in space over areas of aerodynamic significance.

The Mach number correction ΔMa is taken as the value of δMa at one-fourth of mean aerodynamic chord. The α correction is computed from a slightly more elaborated process: it is chord-averaged along the wing span, at three-fourth of local chord, this correction enabling the lift correction to be zero (theory of Pistolesi, [12]).

Second order corrections on drag (buoyancy correction due to velocity distortion) and pitching moment (mainly due to the HTP lift gradient to alpha) are then calculated.

A program called DXV877 has been in used in Onera wind tunnels for two decades to perform the above described computations. Results from this software will be referred as "DXV".

This first approach based on potential equation obviously suffers from some shortcomings:

- the range of validity of the linearized potential equation in terms of Mach number is difficult to appreciate;

- results are applicable to correct upstream Mach number and α, but not the model forces.

In practice, such an approach must always be complemented by experimental twin sting measurement in order to derive a full set of support corrections. In order to investigate the limit of validity of the singularity approach, and to provide more complete correction data, more elaborate simulations of the flow field around the model and support were undertaken and are described in this paper.

3.0 NUMERICAL SIMULATIONS

3.1 Geometry and grids

The wing geometries used for the numerical computations of this study are the ones proposed in the recent DPW-6. They are at scale 1/1 (real aircraft dimensions). The original DPW-5 wing geometry did not match the experimental shape. For DPW-6, the twist and bending data obtained during the CRM campaign in the European Transonic Wind tunnel have been used to generate wing geometries corresponding to different angles of attack. The aero-elastic effects are therefore taken into account.

To perform the RANS computations on these geometries, the meshes "Overset grids Boeing Serrano.REV00" available on the DPW website [3] and the ONERA grids of the horizontal and vertical tails introduced in [13] have been used. The details of the geometries and meshes used are described in [5]. The Z sting mesh has been realized with the software ICEM-CFD (http://www.ansys.com/services/training-center/platform/introduction-to-ansys-icem-cfd-hexa) and the blade sting with the software Pointwise (http://www.pointwise.com). Both meshes are made of about 1.4 million cells. A surface view of the geometries that have been meshed is presented in **Figure 6**. The Z sting line is shorter and more discrete than the blade sting.
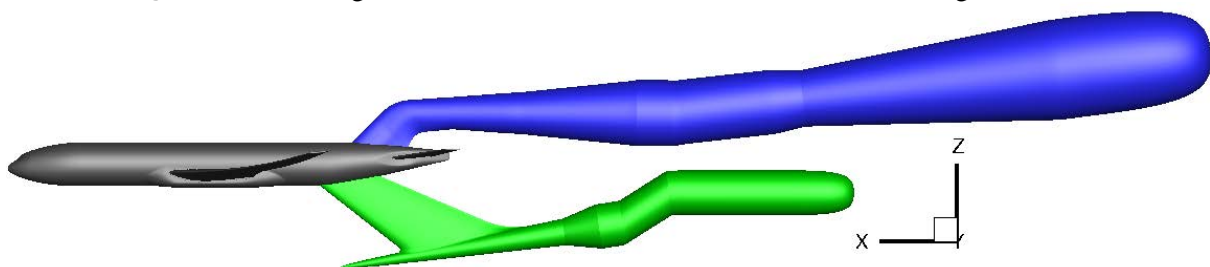
Figure 6: Geometries of the Z sting setup (green) and the blade sting setup (blue).

3.2   ONERA-elsA Reynolds-Averaged Navier-Stokes Solver

All the computations have been performed with elsA [14]. This software uses a cell-centered finite-volume discretization on structured point-matched or Overset grids. In this study, time integration is carried out by a backward-Euler scheme with implicit LU-SSOR relaxation. Spatial discretization is realized using a 2nd order central Jameson scheme [15] with artificial viscosity. Multigrid techniques (one level) are used to accelerate convergence.

Turbulence effects have been simulated with the one-equation Spalart-Allmaras model [16] with the Quadratic Constitutive Relation (QCR) proposed in [17]; it leads to a nonlinear version of the model which does not use the traditional Boussinesq relation anymore.

The Overset interpolations are classically performed over two cell layers around holes and overlap conditions and a double-wall algorithm is used to ensure accurate interpolations when surfaces are described by several grids (collar grid for instance).

The elsA simulations have been executed on a Silicon Graphics cluster (SGI ICE 8200) composed of 5,120 cores representing a power of 57.9 teraflops. The computations carried out for this work have been performed in parallel mode using 48 cores; an 8000-iteration run typically took about 11h.

4.0   METHOD FOR SUPPORT CORRECTION

The first main difficulty arising when considering an aircraft model surrounded by disturbing hardware is to identify a set of equivalent freestream conditions to which one can attribute the measured forces and subsequently make them non dimensional. Like any obstacle, the downstream support generally slows down the flow upstream of itself. Similarly, non-symmetrical devices induce a change in angle of attack on the model. In experiments as in computations, it is therefore necessary to take into account these corrections in Mach number and angle of attack.

4.1   Aerodynamic condition pairing

Let us consider in the **Figure 7** the situation labelled a), which is our reference flow-field without support. The Mach number M_{ref} and angle of attack α_{ref} of the model can be easily defined by looking at flow conditions far upstream from the model. Pressure and force coefficients are defined in a usual way. Let us now consider the situation labelled b), in which the support was introduced. The upstream Mach number and angle of attack are now M' and α'. One first effect of the support is to introduce a change ΔMa in average Mach number and a change $\Delta\alpha$ in angle of attack over the model compared to upstream flow condition. For instance, in the present study the support slows the flow down at model location, so that ΔM is negative. This is standard case for support interference [7][8].

Having this in mind, two different approaches can be followed to derive support interference effects:

- let M' be equal to M_{ref} and α' to α, simulate and compare situation b) to a) in order to derive a support effect under the form of force and pressure increments only;

- or let $M'+\Delta M$ be equal to M_{ref} and $\alpha'+\Delta\alpha$ to α_{ref}, then simulate and compare situation b) to a) to derive force and pressure increment. In this case, the support effect is composed of increments of Mach number, angle of attack, forces and pressure.

In the present study, we adopt the second formulation, arguing that it is close to common wind tunnel definition of the Mach number and AoA which generally includes corrections to cancel mean distortions originating from the support. In fact, ΔM and $\Delta\alpha$ account for mean flow distortion at the model location. If the distortion was homogeneous in space, these corrections would be sufficient to exactly retrieve the reference flow field and forces. Therefore they can be seen as first order correction. The differences in pressure or forces remaining after Mach and angle of attack corrections account for the inhomogeneity of the distortion generated by the support and can be called second order corrections.
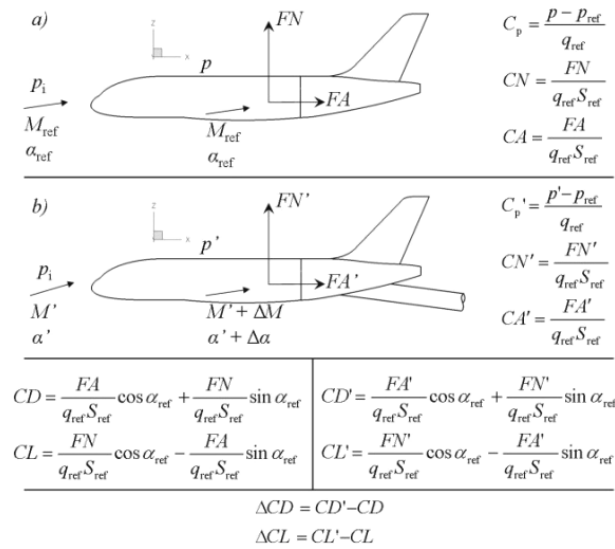
Figure 7: Nomenclature.

One last thing to mention is the use of reference Mach number and angle of attack to compute force and pressure coefficients, for both situation a) and b).

4.2   Determination of upstream flow conditions

It was stated in previous section that ΔM and $\Delta \alpha$ account for mean flow distortion at the model location. In order to implement this definition in practical experiments or computations, one needs to address the notion of 'distortion', 'mean' and 'model location'. Once again, any definition implies a part of arbitrariness, justified by physical or practical considerations.

From the standpoint of linearized potential theory, the idea of distortion is straightforward: it is the velocity generated by singularities associated to the support.

To deal with numerical simulations, let us introduce the following criterion J as the RMS of pressure coefficient distortion on the wing:

$$J = \sqrt{\int_{\text{wing}} \left(C_{\text{p}}{}' - C_{\text{p}} \right)^2 \frac{dS}{S_{\text{wing}}}} \quad \text{(4)}$$

Because Cp' depends on the choice of ΔM and $\Delta \alpha$, J is also a function of ΔM and $\Delta \alpha$. This criterion is expected to be a measurement of the fidelity of the flow with support to the flow without support.
Seeking for a minimum of distortion, let us define:

$$\left(\Delta Ma, \Delta \alpha \right) = \arg \min \left(J \right) \quad \text{(5)}$$

With this definition, first order corrections (ΔM, $\Delta \alpha$) are found after a minimization process.

5.0   APPLICATION TO WIND TUNNEL TESTS

This methodology has been validated against experimental twin sting measurements available for another model before applying it to any wind tunnel test campaigns.

5.1   First order corrections

In order to identify the corrections defined by Eq.5, the (ΔM, $\Delta \alpha$) space is sampled until the optimum is identified with sufficient accuracy. From the sampled values, the J-criterion was interpolated by Kriging method to produce **Figure 8** and **Figure 11**. A qualitative analysis of the obtained database reveals that J is

mainly a sensor for the shock wave position, which is mainly driven by the Mach number in the flow condition under study and for this wing design. It explains why the *J*-criterion is much more sensitive to this variable. Like on most transonic airfoil at design point, the shock wave moves downstream when the Mach number or angle of attack increases. We choose to find the optimum corrections at cruise point, then to keep those values for the whole polar.

5.1.1   S1MA

For the S1MA Z sting setup, J-criterion leads to an optimum ($\Delta M = -0.003$, $\Delta\alpha = 0.02$), as shown in **Figure 8**. We choose to pick the smallest Mach number correction as the criterion isn't really sensitive to the angle of attack. As expected, the angle of attack correction is positive as the support generates upwash near the model.
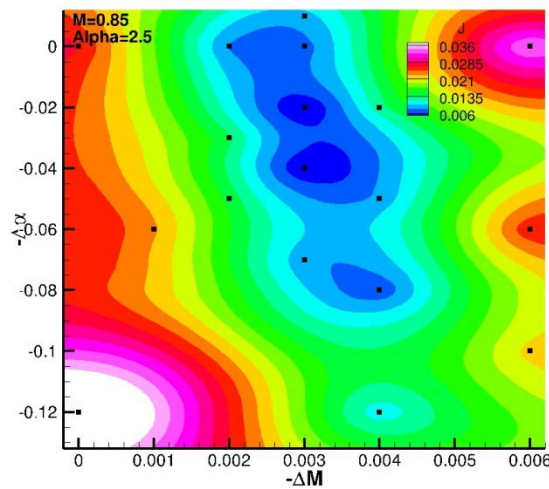
Figure 8: RMS of wing pressure distribution with Z-sting for various *ΔM* and *Δα*. Dots indicate sampled points. Reference flow condition is Ma=0.85, α=2.5°.

Even with minimal distortion, a RMS-averaged residual discrepancy of around 0.004 in pressure coefficient remains on the wing, most of which originates from the shock wave area, since the shock position and intensity cannot be exactly reproduced on the whole span when sting is installed, as depicted in **Figure 9**. We clearly see that without any first order corrections, the shock position on the wing isn't at the same place with and without the sting.
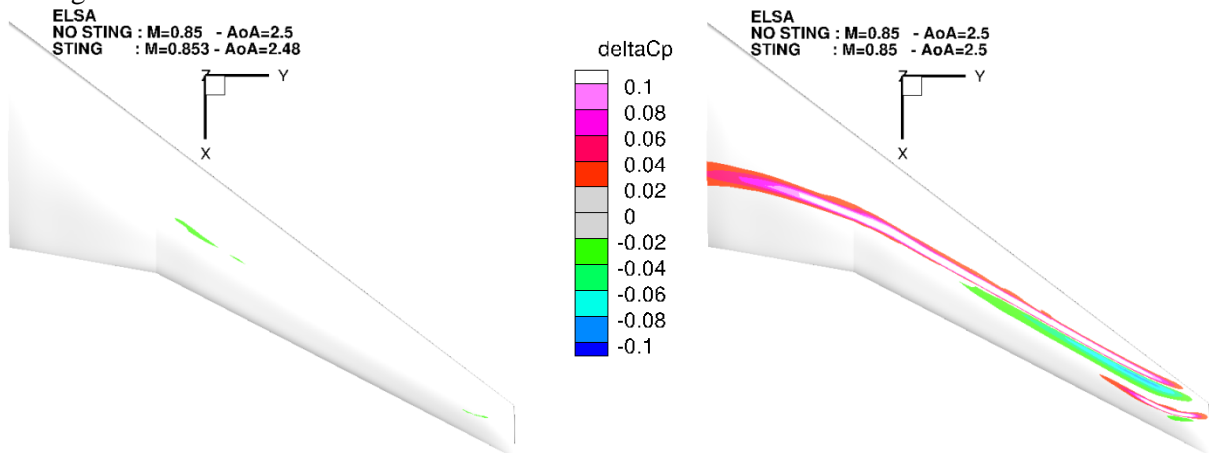
Figure 9: Pressure coefficient disturbance with Z sting on the wing for the optimum J-criterion (left) and without corrections (right) at Ma=0.85 and α=2.5°.

At lower and higher angle of attack, this optimum leads to limited impact on the wing only visible at the shock position as shown in **Figure 10**.
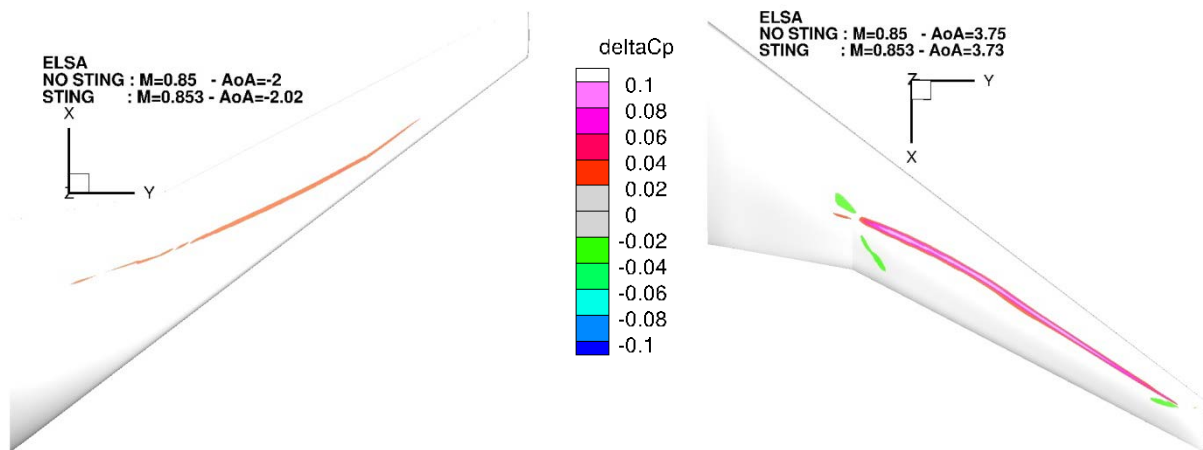
Figure 10: Pressure coefficient disturbance with Z sting on the wing at Ma=0.85 and α=-2° (left, pressure side showed) and α=3.75° (right, suction side showed).

5.1.2   NTF-Ames-ETW

For the blade sting setup, J-criterion leads to an optimum (ΔM = −0.004, Δα = -0.05), as shown in **Figure 11**. We choose to pick the smallest Mach number correction as the criterion isn't really sensitive to the angle of attack. As expected, the angle of attack correction is negative as the support generates downwash near the model.
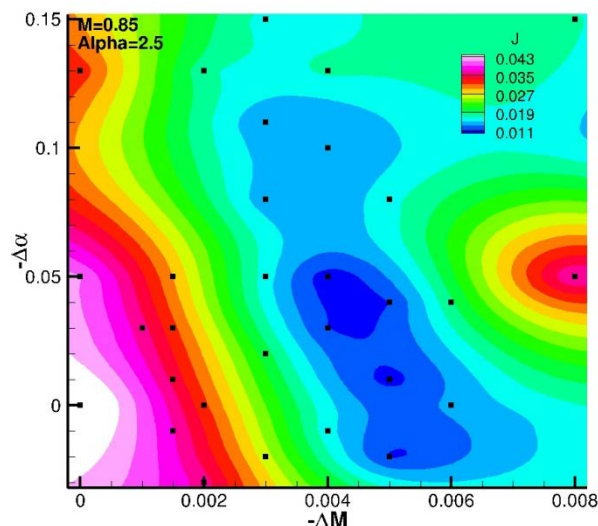
Figure 11: RMS of wing pressure distribution with blade sting for various ΔM and Δα. Dots indicate sampled points. Reference flow condition is Ma=0.85, α=2.5°.

A RMS-averaged residual discrepancy of around 0.009 in pressure coefficient remains on the wing. The pairing process was harder to obtain than with the Z sting, and the remaining flow disturbance on the wing is higher, as it can be seen on **Figure 12**. It can also be seen that without correction, the blade sting generates more disturbance than the Z sting.
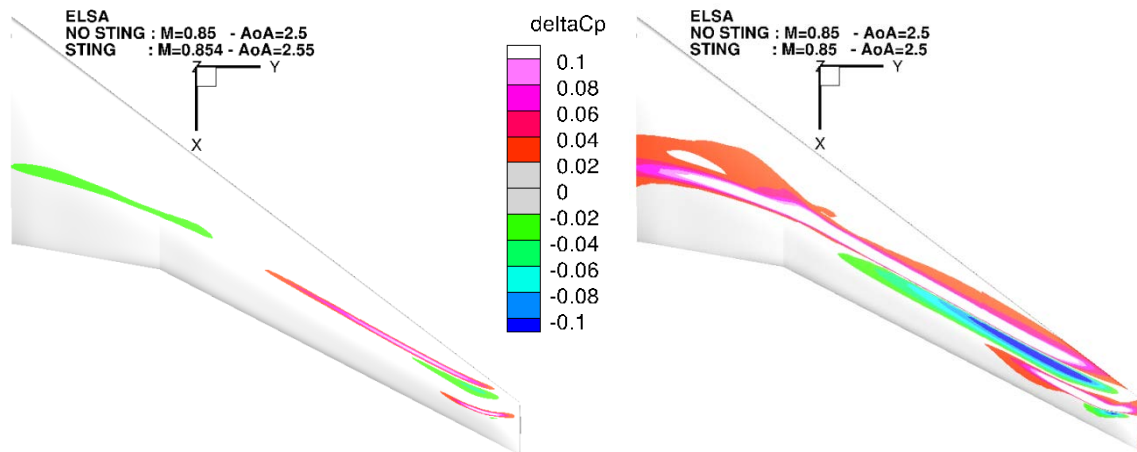
Figure 12: Pressure coefficient disturbance with blade sting on the wing for the optimum J-criterion (left) and without corrections (right) at Ma=0.85 and α=2.5°.

At higher angle of attack, this optimum leads to limited impact on the wing only visible at the shock position as shown in **Figure 13**. At lower angle of attack, the impact on the wing is higher than the Z sting set up.
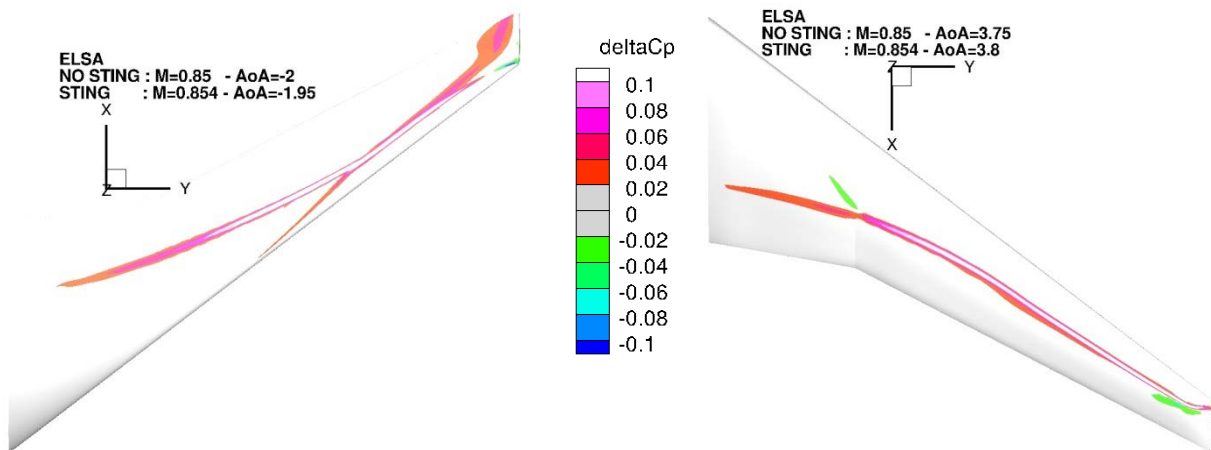
Figure 13: Pressure coefficient disturbance with blade sting on the wing at Ma=0.85 and α=-2° (left, pressure side showed) and α=3.75° (right, suction side showed).

5.2   Second order corrections

5.2.1   Pressure

Flow distortion generated by the stings can be observed on **Figure 14** that displays pressure coefficient disturbance on the model skin. The pairing process logically leads to perturbations limited to the rear part of the model. Main perturbations are located on the rear fuselage and the HTP. The effective local incidence on the HTP is modified by the sting, which is visible on the HTP lifting surface.
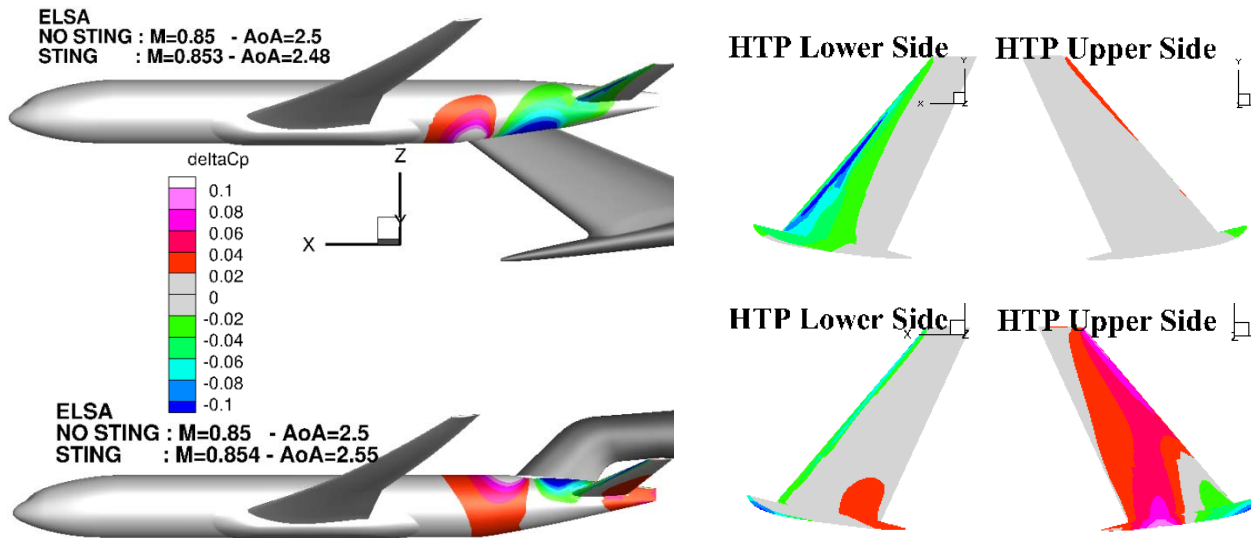
Figure 14: Pressure coefficient disturbance on the model with Z sting (top) and blade sting (bottom) at Ma=0.85 and α=2.5°.

5.2.2   Force and moment

Comparison of Z sting and blade sting effect on forces is carried out in **Figure 15** for *Ma*=0.85. The support effect on wing lift is of weak order of magnitude (less than 0.002) but there is still a residual difference in the wing drag of about +4 drag counts for both stings (1 drag count = 10^{-4}). The most significant difference of the sting effect on drag (presented in body axes) comes from the body where the effects are off opposite sign (with the same order of magnitude in absolute). Adding all the contributions, the effect of Z sting on drag is of limited amplitude (about -8 drag counts) but is much larger with the blade sting with about 25 drag counts. This is mainly due to compensation between body, HTP and wing for the Z sting whereas the effects do not compensate with the blade sting.

Concerning the lift, the effects come mainly from the HTP and also the body for the blade sting. For the pitching moment, it indeed comes mainly from the HTP. The total effect on pitching moment is almost twice bigger with the blade sting than with the Z sting.

Globally, the trend with angle of attack is quite linear up to CZ=0.5, but a noticeable trend change occurs for CZ>0.52 which can be correlated to the apparition of flow separation on the wing upper side.
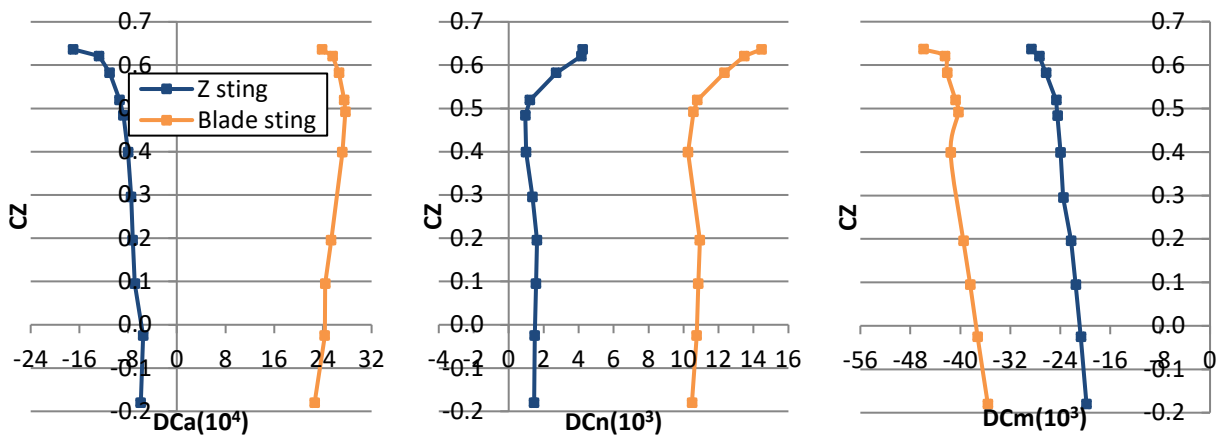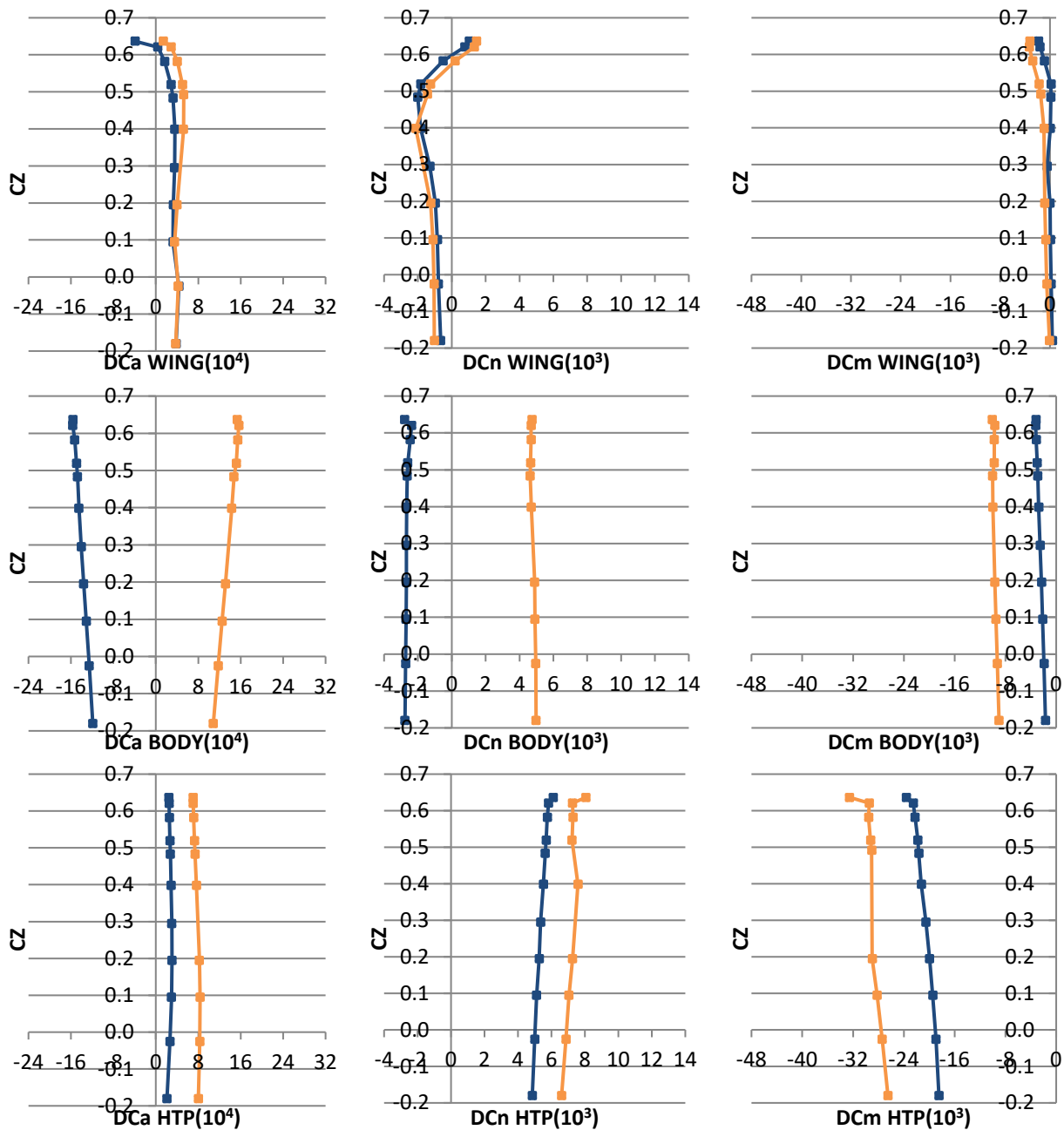
Figure 15: Force increments due to Z sting and blade sting at *Ma*=0.85, on the complete model, one the wing, on the body and on the HTP.

5.3 Comparison between wind tunnels

One major objective of this paper is to compare the data between the NASA wind tunnels, ETW and S1MA, and more specifically global coefficients. No pressure distributions are available from the CRM model apart from the wing so no comparison can be made. Comparisons on the wing are addressed in [5]. This is a crucial step for absolute performance prediction and code validation. The comparison is made on the WBH configuration for which results are available in all wind tunnels. The data presented here were obtained at a Mach number of 0.85 and a chord Reynolds number of 5 million. Transition was fixed for all wind tunnel tests (also at 10% chord).

5.3.1 Drag

The drag polar obtained on the WBH configuration at $Ma = 0.85$ is first examined. **Figure 16** shows the comparison between the four wind tunnels, with the previous calculated support corrections for S1MA, NASA and ETW tests. Farfield support corrections applied by ETW have been added. These results are not corrected for near-field effects using CFD computations but only for far-field effects using the Long Axial Probe calibration.

First, all NASA and ETW results are similar if not corrected for support effects (dashed lines). The same support was used for these three tests. It notably shows that wall corrections are well taken into account.

Then, the comparison between the corrected results is rather good. The ETW results corrected for far-field and near-field effects show a difference of about 5 d.c at cruise point. Indeed, a drag difference of less than 5 d.c. is observed between all corrected wind tunnels at CL = 0.1. And, most important, at design point, a difference of 5 d.c. appears.
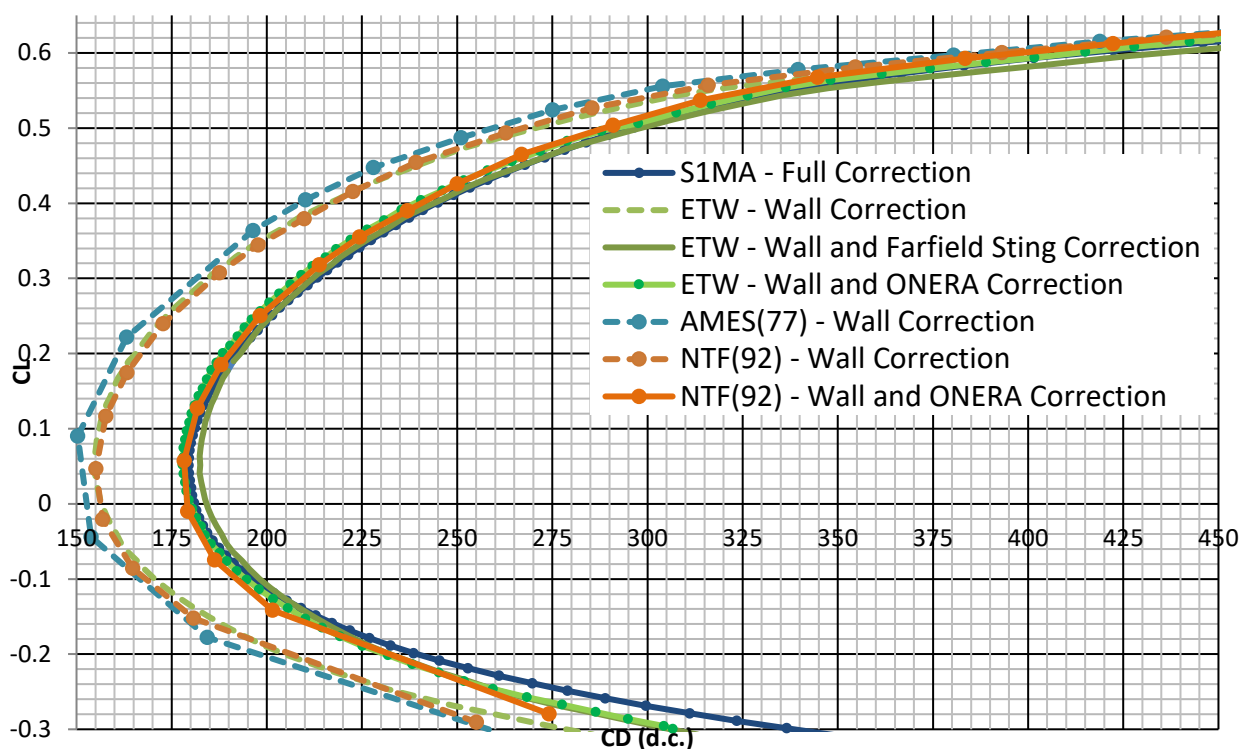
Figure 16: Drag polar at *Ma*=0.85.

5.3.2 Pitching moment

The pitching moment variation with lift is examined in **Figure 17**.

First, the wind tunnels which are not corrected for support effect show consistent results. Then, the farfield sting corrections from ETW do not include any pitching moment correction. As presented in [18] and calculated in the previous section, the blade sting support effect calculated by CFD shows an increase of pitching moment $\Delta CM = 0.036$ at a lift coefficient around 0.4. This significantly reduces the discrepancies between S1MA and NTF/AMES/ETW data as depicted by the increment on the pitching moment in **Figure 17**.
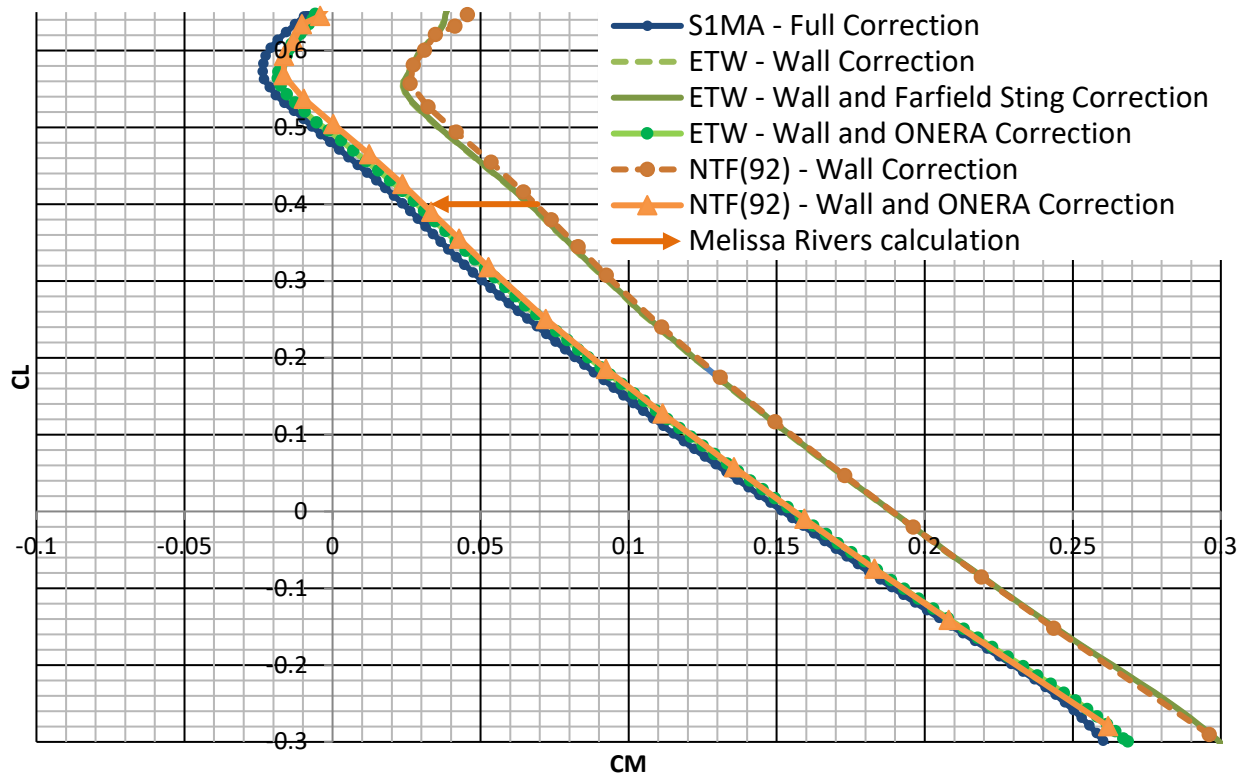
Figure 17: Pitching moment at *Ma*=0.85.

6.0 CONCLUSION

The article is focused on the comparisons between experimental results of the CRM and LRM results that have been obtained in several wind tunnels. For this matter, high fidelity CFD method has been applied to calculate support interference effects. Special attention was paid to the proper deviation of corrections of the incoming flow conditions in terms of Mach number and angle of attack. These support effects have been considered as increments; allowing experimental results from different wind tunnels and support system to be compared. The remaining discrepancies between the fully corrected results have been reduced, leading to better comparison between wind tunnels. Additional calculations have to be carried out particularly at high lift to complete the corrections.

7.0 AKNOWLEDGMENTS

The authors would like to thank the ONERA-S1MA team. They also thank the DPW organising committee and Melissa Rivers, who give us the CAD of the CRM model support. The numerical studies presented in this article have been performed with the software elsA which is co-owned by AIRBUS, SAFRAN, and ONERA (ASO).

8.0   REFERENCES

[1] Vassberg, J. C., DeHann, M. A., Rivers, S. M., and Wahls, R. A., "Development of a Common Research Model for Applied CFD Validation Studies," AIAA Paper 2008-6919, 2008.

[2] NASA, Langley Research Center, "Common Research Model", http://commonresearchmodel.larc.nasa.gov/.

[3] DPW-6 website, http://aiaa-dpw.larc.nasa.gov/.

[4] ONERA website, http://windtunnel.onera.fr/s1ma-continuous-flow-wind-tunnel-atmospheric-mach-005-mach-1.

[5] Cartieri, A., Hue, D., Chanzy, Q., and Atinault, A., "Experimental Investigations on the Common Research Model at ONERA-S1MA-Drag Prediction Workshop Numerical Results," *Journal of Aircraft*, July 2017, doi: 10.2514/1.C034414.

[6] Website ESWIRP for ETW data, http://www.eswirp.eu/ETW-TNA-Dissemination.html.

[7] Heidebrecht, A., "Simulation and Model Support Corrections for Slotted Wall Transonic Wind Tunnels", *AAAF Wind tunnel and computation: a joint strategy for flow prediction*, FP20, AAAF, Paris, March 2012.

[8] Cartieri, A., and Mouton, S., "Using CFD to calculate support interference effects", *28th AIAA Aerodynamic Measurement Technology, Ground Testing, and Flight Testing Conference*, AIAA Paper 2012-2864, 2012.

[9] Rivers, M., "Comparison of the NASA Common Research Model European Transonic Wind Tunnel Test Data to NASA Test Data", *5th CEAS Air and Space Conference,* CEAS Paper 2015-161, 2015.

[10] Le Sant, Y., Mignosi, A., Touron, G., Deléglise, B., Bourguignon, G., "Model Deformation Measurement (MΔM) at ONERA", *25th AIAA Applied Aerodynamics Conference*, AIAA Paper 2007-3817, June 2007.

[11] Vaucheret X., "Recent Calculation Progress on Wall Interferences in Industrial Wind Tunnels", *La Recherche Aérospatiale*, No. 3, 1988, pp 45-47.

[12] Pistolesi, E., "*Collected lectures of the principal meeting of the Lilienthal society*", Considering respecting the mutual influence of system of airfoils, Berlin, Germany, 1937, pp. 214-219.

[13] Hue, D., Péron, S.,Wiart, L., Atinault, O., Gournay, E., Raud, P., Benoit, C., and Mayeur, J., "Validation of a Near-Body and Off-Body Grid Partitioning Methodology for Aircraft Aerodynamic Performance Prediction", *Computers and Fluids Journal*, Vol. 117, Aug. 2015, pp. 196–211, doi:10.1016/j.compfluid.2015.05.021.

[14] Cambier, L., Heib, S., and Plot, S., "The ONERA elsA CFD Software: Input from Research and Feedback from Industry," *Mechanics and Industry*, Vol. 14, No. 3, 2013, pp. 159–174, doi:10.1051/meca/2013056.

[15] Jameson, A., Schmidt, W., and Turkel, E., "Numerical Solution of the Euler Equations by Finite Volume Methods Using Runge–Kutta Time Stepping Schemes," AIAA Paper 1981-1259, June 1981.

[16] Spalart, P. R., and Allmaras, S. R., "AOne-Equation Turbulence Model for Aerodynamic Flows," AIAA Paper 1992-0439, 1992.

[17] Spalart, P. R., "Strategies for Turbulence Modelling and Simulation", *International Journal of Heat and Fluid Flow*, Vol. 21, No. 3, 2000, pp. 252–263, doi:10.1016/S0142-727X(00)00007-2.

[18] Rivers,M. B., Hunter,C. A., and Campbell, R. L., "Further Investigation of the Support System Effects and Wing Twist on the NASA Common Research Model," AIAA Paper 2012-3209, 2012.